Check for updates

Adsorption mechanism of aqueous Cr(VI) by Vietnamese corncob biochar: a spectroscopic study†

Duy-Khoi Nguyen, [a] Quoc-Bao Ly-Tran,[a] Van-Phuc Dinh, [*a] Bich-Ngoc Duong,[a] Thi-Phuong-Tu Nguyen[a] and Pham Nguyen Kim Tuyen[b]

Cr(VI) is highly toxic and carcinogenic, posing significant threats to health and ecosystems. This study utilizes solid waste from corncobs to synthesize biochar (CCBC) for the removal of Cr(VI) from water. The most effective Cr(VI) removal was achieved at pH 2.0, with a maximum adsorption capacity (Q_m, Langmuir, mg g^{-1}) of 38.1, higher than that of activated carbon (25.69), composite (35.84), and magnetic biochar (25.94) derived from corncobs. Brunauer–Emmett–Teller (BET) results indicated that Cr(VI) was adsorbed on the internal surface instead of external surface. Scanning electron microscope (SEM-mapping) images combined with the pH$_{PZC}$ value (7.6) demonstrated that Cr(VI) interacts with the material surface *via* electrostatic mechanisms. Energy-dispersive X-ray (EDX) spectra combined with Fourier-transform infrared (FTIR) spectra demonstrate that two key adsorption mechanisms in this study are surface adsorption (Cr(VI)-biochar) followed by the reduction of Cr(VI) to Cr(III), allowing ion exchange adsorption to occur. X-ray diffraction (XRD) patterns indicate no precipitation on the surface, and the material remains stable after four reuse cycles. These results suggest that CCBC can be used as an efficient, cost-effective, and environmentally friendly adsorbent for Cr(VI) removal from water. This is the first study to combine spectroscopic methods and theoretical models to gain deeper insights into the Cr(VI) adsorption mechanisms onto CCBC.

1. Introduction

Water pollution caused by heavy metals can lead to serious health issues for humans and disrupt ecological balance.[1] Heavy metals enter water sources through industrial activities such as electroplating, battery production, fertilizers, mining, and chemicals.[2,3] For example, at very low concentrations (1 μg L^{-1}), Pb(II) ions can impair children's memory.[4] Meanwhile, prolonged exposure and work in environments containing Cr(VI), Ni(II), and Cd(II) are major causes of lung, nasal, and skin cancers.[5,6] Among these metals, Cr(VI) has been classified as a carcinogen by environmental and health organizations such as IARC, EPA, and WHO, with a maximum allowable concentration in drinking water of 50 μg L^{-1}.[7] Therefore, research on the treatment of Cr(VI) in aqueous solutions holds significant practical importance. Many physicochemical methods have been studied for the treatment of Cr(VI) in water, including adsorption;[8] nanofiltration;[9] ultrafiltration and reduction;[10] complexation;[11] chemical coagulation/electrocoagulation;[12] electrochemical reduction/oxidation;[13] electrodeionization;[14] and ion exchange.[15] Among the aforementioned physicochemical methods, adsorption offers several advantages such as simplicity in execution, high efficiency, and low investment cost.[6]

Biochar is known as a low-cost, environmentally friendly adsorbent material capable of treating water pollution caused by heavy metals,[16] dyes,[17] and radioactive substances.[18] Therefore, research on biochar and its applications in environmental remediation has garnered significant interest from scientists.[19] Especially, the use of biochar derived from agricultural by-products is not only environmentally beneficial by utilizing a large amount of agricultural waste but also economically advantageous due to the abundant and stable supply of raw materials. Additionally, the energy required to convert biomass into biochar is minimal since the reaction occurs at low temperatures. Among agricultural wastes, corn is one of the most commonly consumed foods in many countries around the world,[20] resulting in a large amount of corncobs being discarded into the environment daily. Therefore, the use of corncobs as a raw material for synthesizing new materials to treat Cr(VI) from aqueous solution has attracted many scientists. For instance, in 2018, H. Li *et al.* modified biochar from corncobs with H_3PO_4 to create activated carbon for Cr(VI) adsorption.[21] The results showed that the maximum adsorption capacity (Q_m) of the material was relatively low, approximately 9.9 mg g^{-1}. Also in 2018, G. K. Gupta *et al.* used activated carbon from corncobs to adsorb Cr(VI) with a $Q_m = 5$ mg g^{-1}.[22] O. Xin *et al.*

[a]*Institute of Interdisciplinary Social Sciences, Nguyen Tat Thanh University, Ho Chi Minh City, 700000, Vietnam. E-mail: dvphuc@ntt.edu.vn*

[b]*Faculty of Environment, Sai Gon University, Ho Chi Minh City 700000, Vietnam*

and L. P. Hoang *et al.* studied the removal of Cr(vi) using Fe_2O_3/corncob biochar magnetic composites, with Q_m of 61.97 and 25.94 mg g^{-1}, respectively.[23,24] Y. Yang *et al.* (2018) utilized polypyrrole/corncob magnetic composites to remove Cr(vi) through combined adsorption and reduction, achieving a Q_m of 19.23 mg g^{-1}.[25] However, research on Cr(vi) adsorption using corncob biochar remains limited compared to activated carbon or composites. In 2023, a publication reported the Cr(vi) removal capacity of corncob biochar with a Q_m of 25 mg g^{-1},[26] this value is significantly higher than that of biochar/activated carbon synthesized from durian shell (Q_m = 6.66 and 7.58 mg g^{-1}, respectively);[27] oak wood biochar (3.03 mg g^{-1});[28] oak shell (4.62 mg g^{-1});[28] and animal bone (8.4 mg g^{-1}).[29] Specifically, the research indicates that the adsorption of Cr(vi) is enhanced by the presence of silicon (Si) in the form of amorphous hydrated silica found in Si-rich plants, including corn.[30,31] This indicates the potential of corncob biochar in treating water pollution caused by heavy metal Cr(vi).

In this study, we utilized corncob by-products to synthesize biochar for the adsorption of Cr(vi) in aqueous solutions. The optimal conditions for biochar synthesis were selected based on the evaluation of Cr(vi) adsorption capacity under various temperature and time conditions. Physicochemical analysis methods, including XRD, SEM-EDX-mapping, BET, and FTIR, were employed to assess the adsorption mechanism of Cr(vi) in water. The corncob-derived biochar demonstrated effective Cr(vi) removal in aqueous solutions, contributing to the development of an environmentally friendly and economically viable adsorbent for practical applications.

2. Experimental methods

2.1. Chemicals

Corncobs are collected at markets, supermarkets, and restaurants in Ho Chi Minh City, Vietnam. $K_2Cr_2O_7$ (>99.9%), $K_2Cr_2O_7$ standard solution 1000 mg L^{-1}, HNO_3 (65%), NaOH pellets (>99%), KCl (99%) were purchased from Merck company. No additional purification was carried out of these chemicals unless otherwise specified. A Barnstead Easypure II ion-exchange system provided deionized water (DI) with a resistivity of 16.4 MΩ·cm.

2.2. Characterization of biochar

The structure of the biochar was analyzed using XRD. The analysis was performed on a Bruker D8 Advance, CuKα (λ = 1.54178 Å) (Billerica, MA, USA), with a scanning angle 5–50°,

and a scanning speed of 0.02° s^{-1}. The surface area of the material was determined by N_2 adsorption–desorption measurements at −196 °C on a Micromeritics 3Flex (USA). The surface morphology of the material was analyzed by SEM on an S-4800 (Hitachi, Japan) combined with EDX spectroscopy to determine the chemical composition of the material. Functional groups and characteristic vibrations of the material were analyzed by FTIR spectroscopy on an FTIR-4X (Jasco, Japan) in the range of 400–4000 cm^{-1} using the KBr pellet method.

2.3. Synthesis of biochar

The synthesis process of biochar material from corncobs is presented in Scheme 1. Specifically, after collection, the corncobs were washed with distilled water, cut into small pieces (2 cm × 2 cm × 2 cm), and dried at 100 °C until a constant weight was achieved (1). The dried corncobs were then pyrolyzed at 500, 600, and 700 °C for 15, 30, and 45 min under anoxic conditions to obtain biochar (2). The biochar was washed several times with distilled water, dried, and finely ground to obtain powdered CCBC (3).

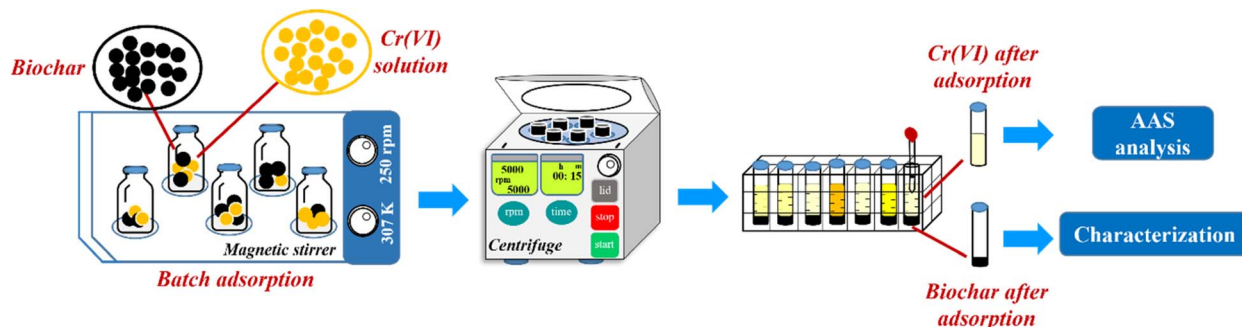## 2.4. Adsorption of Cr(vi) by corncob biochar

2.4.1. Determining the point of zero charge (pH$_{pzc}$).
In this study, the salt addition method was used to determine the point of zero charge (pH$_{pzc}$) of corncob biochar.[32] Specifically, 50 mL of 0.1 M KCl solution (initial pH, pH$_i$ = 2–12) containing 0.1 g of CCBC material was added to each beaker and stirred for 24 hours at room temperature. The solution was then filtered, and the pH value (final pH, pH$_f$) was measured. The Δ_{pH} value (Δ_{pH} = pH$_f$ − pH$_i$) was calculated. The point of zero charge (pH$_{pzc}$) was determined through the relationship between pH$_i$ and Δ_{pH}.[32]

2.4.2. Investigation of factors influencing the adsorption process.
In this study, the factors affecting the adsorption of Cr(vi) on corncob biochar were investigated, including pH (2–11); adsorption time (5–270 minutes); initial Cr(vi) concentration (25–225 mg L^{-1}); adsorption dosage (0.05–0.125 g); and competing ion strength (KCl 0.0–18.63 × 10^3 mg L^{-1}). The adsorption process was carried out according to the procedure presented in Scheme 2. Specifically, 50 mL of Cr(vi) solution was added to a 100 mL glass flask containing 0.1 g of CCBC, and stirred at 250 rpm using a 10-point magnetic stirrer RSM-03-10K (Phoenix Instrument, Germany) at 34 °C. After adsorption, the samples were centrifuged at 6000 rpm for 30 minutes to separate the biochar from the Cr(vi) solution. The concentration of
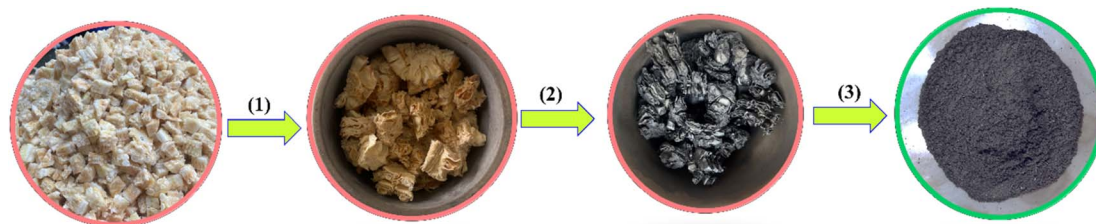
Scheme 1 The procedure for synthesizing corncob biochar.

Scheme 2 Cr(VI) adsorption experiment onto corncob biochar.

Cr(VI) before and after adsorption was determined using atomic absorption spectroscopy (AAS) on a ZA3300 device (Hitachi, Japan). Each adsorption experiment was performed three times to calculate the standard deviation and error.

Removal efficiency (% removal) and adsorption capacity (Q_e, mg g^{-1}) were determined according to eqn (1) and (2), respectively:[33]

$$\text{Removal efficiency} = \frac{C_0 - C_e}{C_0} \times 100\ \% \quad (1)$$

$$Q_e = \frac{C_0 - C_e}{m} \times V \quad (2)$$

where C_0 (mg L^{-1}) and C_e (mg L^{-1}) are the initial and final concentrations of Cr(VI) solution respectively; V (L) is the volume of the Cr(VI) solution used for adsorption, and m (g) is the weight of adsorbent used.

2.4.3. Investigation of isotherm and kinetic models. Four isotherm models and four nonlinear kinetic models were used to study the isotherm and kinetic adsorption properties. Specifically, the four isotherm models used were: Langmuir, Freundlich, Sips, and Redlich–Peterson. The four kinetic models included: pseudo-first-order kinetics, pseudo-second-order kinetics, intraparticle diffusion kinetics, and Elovich kinetics (Table S1†).

2.4.4. Data analysis. In this study, to evaluate the influence of factors (pH, sorbent dosage, ionic strength and contact time) on the adsorption capacity of this material, ANOVA: single factor analysis was calculated using Excel software. Results of ANOVA analysis was shown in ESI.†

Besides, we used nonlinear methods to determine the parameters of isotherm and kinetic models. To assess the accuracy of these models, we calculated the Root Mean Square Error (RMSE) and chi-square (χ^2) error functions. These error metrics are defined as follows:

$$\text{RMSE} = \sqrt{\frac{1}{(n-1)} \sum_{n=1}^{n} \left(Q_{e,meas} - Q_{e,calc}\right)^2}, \quad (3)$$

$$\chi^2 = \sum_{n=1}^{n} \frac{\left(Q_{e,meas} - Q_{e,calc}\right)^2}{Q_{e,calc}}, \quad (4)$$

In these equations, $Q_{e,meas}$ and $Q_{e,calc}$ represent the experimentally measured and theoretically calculated adsorption capacities, respectively. We employed the Solver add-in function in Microsoft Excel to determine these values using the least-squares method. Lower RMSE and χ^2 values indicate a better fit between the experimental data and the theoretical model, and the lowest values signifying the best-fitting model.

2.5. Desorption and recycle of corncob biochar

In this study, the desorption and reuse capabilities of biochar material derived from corncobs were investigated. For desorption, after Cr(VI) adsorption, the biochar was stirred in NaOH solutions with increasing concentrations from 0.1 to 0.9 M for 60 minutes to evaluate desorption efficiency. After desorption, the biochar material was washed multiple times with distilled water until the wash water reached a neutral pH. The washing process was performed by centrifugation at 6000 rpm for 30 minutes. The material was dried at 100 °C until a constant weight was achieved, then subjected to a second Cr(VI) adsorption. The desorption and reuse process was repeated for 4 cycles. The procedural scheme is presented in Scheme S1.†

3. Results and discussion

3.1. Effect of pyrolysis condition

To investigate the impact of pyrolysis conditions on the conversion of corncob biomass into biochar, the pyrolysis process was conducted at temperatures of 500, 600, and 700 °C for durations of 15, 30, and 45 minutes. Published studies have shown that biochar derived from corncobs synthesized through pyrolysis, typically performed within the temperature range of 500–700 °C, exhibits the best capability for Cr(VI) removal. For instance, H. Li *et al.* conducted the carbonization of corncobs at 400–500 °C, and the material obtained from the carbonization process at 500 °C exhibited the most effective Cr(VI) adsorption capacity.[21] O. Xin *et al.* reported that CCBC synthesized at 650 °C had the highest maximum adsorption capacity according to the Langmuir model (61.79 mg g^{-1}).[23] Meanwhile, A. Shakya *et al.* indicated that CCBC synthesized at temperatures ranging from 350 to 650 °C could adsorb 100% of 50 mg per L Cr(VI), with the CCBC synthesized at 350 °C showing the highest maximum adsorption capacity according to the Langmuir model (65.75 mg g^{-1}).[26]
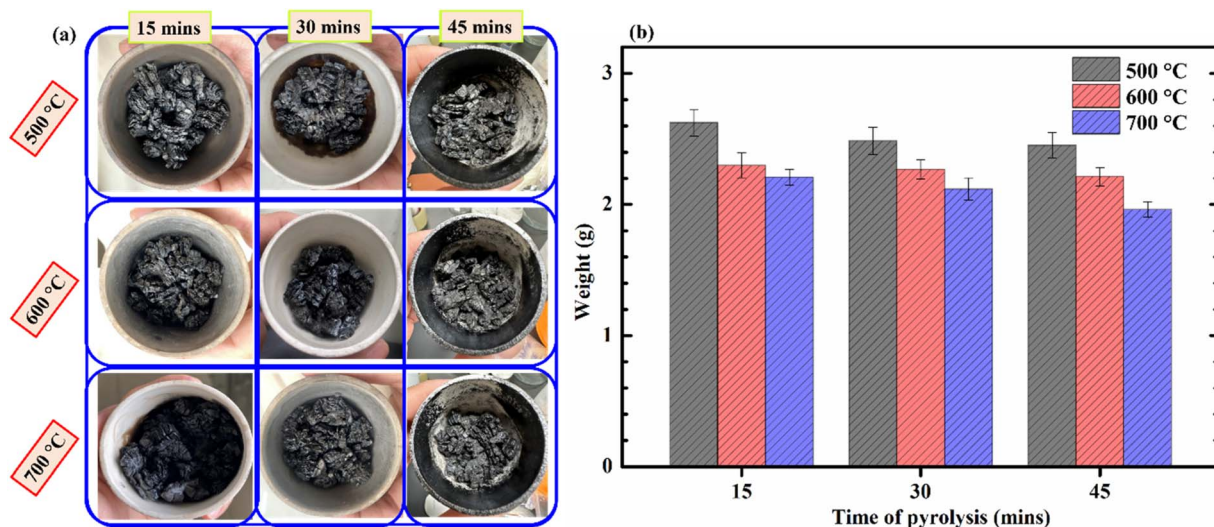
Fig. 1 Biochar products from corncobs (a); and the mass variation of biochar (b) under different pyrolysis conditions.

The images of corncobs after pyrolysis under different conditions are presented in Fig. 1a, and the mass of the obtained products is shown in Fig. 1b. It can be observed that under nine different pyrolysis conditions, the materials obtained all exhibit the characteristic black color of biochar. The mass of the obtained products decreases with increasing temperature and pyrolysis time. This indicates that the conversion process from biomass to biochar is more efficient at higher temperatures or with extended duration at the same pyrolysis temperature. Table S2† presents the efficiency of the biochar synthesis process from corncobs. From Table S2,† it can be observed that the conversion efficiency of corncobs to biochar ranges from approximately 26% to 20% within the temperature range of 500–700 °C. Temperature has a greater impact on efficiency compared to pyrolysis time. For instance, increasing the pyrolysis temperature from 500 to 600 °C over the same duration of 15 minutes results in a decrease in efficiency by about 3.5%. Meanwhile, extending the duration from 15 to 45 minutes at the same temperature of 500 °C only reduces efficiency by approximately 1.8%. These results are quite consistent with the findings of several authors regarding the optimal temperature range for synthesizing biochar from corncobs (approximately 350–700 °C).[21,23] As the pyrolysis temperature increases, the synthesis yield gradually decreases. This can be explained by the fact that at high pyrolysis temperatures, various reactions occur within the corncob. Compounds in the biomass decompose, such as water, and organic compounds transform into gases, leading to a reduction in synthesis yield. A similar trend was observed in the study of biochar synthesis from corncobs by G. K. Gupta et al.,[22] and from Leucaena leucocephala bark by K. Anupam et al.[34] Studies also indicate that at temperatures above 500 °C, the slow decomposition of lignin compounds primarily occurs, playing a major role in the synthesis yield of biochar.[35]

The analyzed results indicate that pyrolysis time has minimal impact on the synthesis efficiency. In contrast, pyrolysis temperature has a more pronounced effect. Consequently, we selected three samples, CCBC-500-15, CCBC-600-15, and CCBC-700-15, to analyze certain material characteristics.

3.2. Biochar characterization

3.2.1 BET analysis. The effect of pyrolysis temperature on the porosity of CCBC material is presented in Fig. 2a and b. According to the IUPAC classification of adsorption isotherms, the sample pyrolyzed at 500 °C exhibits a type I isotherm (microporous)[36] while those pyrolyzed at 600–700 °C exhibit a type IV (mesoporous) isotherm.[37] Indeed, Fig. 2b shows that the corncob sample pyrolyzed at 600–700 °C exhibits hysteresis in the N_2 desorption isotherm in the relative pressure region $P/P_0 > 0.5$, which is explained by the condensation of N_2 in mesopores. The hysteresis loop reflects a complex porous structure and may be a combination of several typical pore shapes such as bottle-shaped and tubular pores with uneven pore size distribution.[37] The porosity of CCBC pyrolyzed at 500–700 °C is presented in Table S3.† Accordingly, as the pyrolysis temperature increases, the surface area and pore volume of CCBC significantly increase. Specifically, at the highest pyrolysis temperature of 700 °C, the material has a surface area and pore volume of 443 m^2 g^{-1} and 0.194 cm^3 g^{-1}, respectively. These values are higher compared to activated carbon from corncob synthesized by other authors. Additionally, they are also higher than some biochars synthesized from common by-products such as cassava stems,[38] bagasse,[39] pomelo peels.[16] This indicates the potential application of CCBC in environmental pollution treatment through adsorption methods.

3.2.2 XRD analysis. Fig. 2c presents the XRD patterns of corncob samples pyrolyzed at 500–700 °C. Observing Fig. 2c, it is evident that all three samples corresponding to the three pyrolysis temperatures exhibit similar XRD patterns with diffraction peaks characteristic of biochar structures. Specifically, the amorphous carbon structure of the biochar material can be observed at the diffraction angle of 22–25° (ref. 16) and
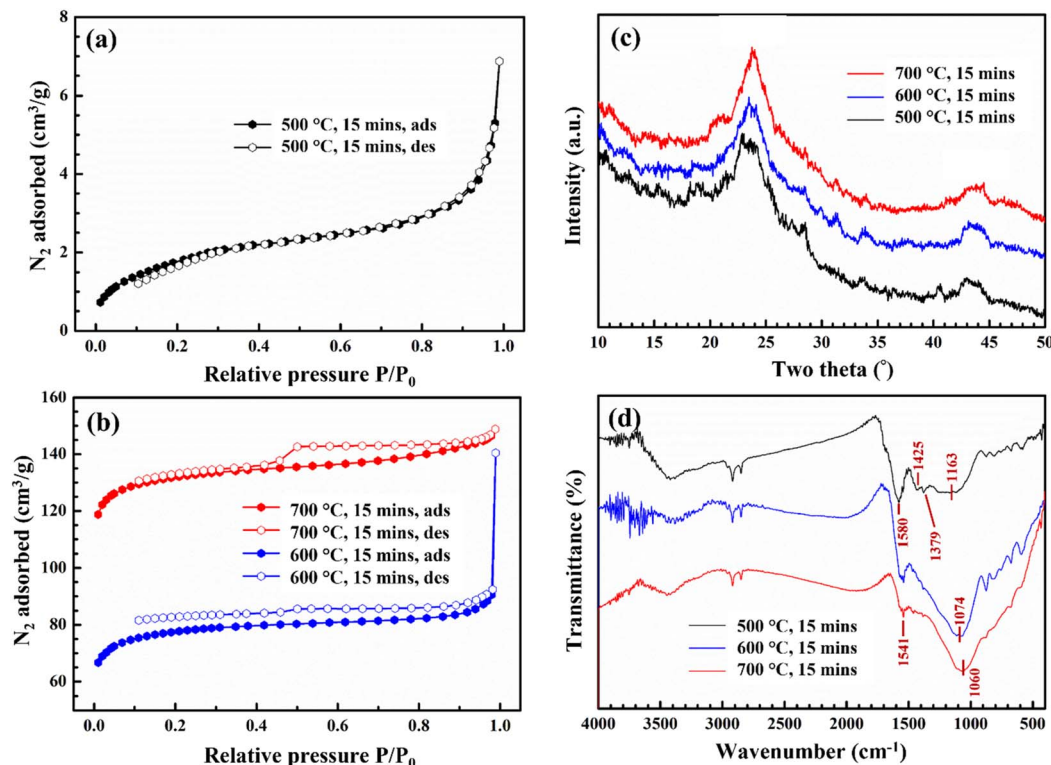
Fig. 2 Characterization of CCBC: BET (a and b); XRD patterns (c); and FTIR spectra (d).

the graphite structure at the diffraction angle of 41–43°.[40] Thus, combining the XRD and BET results, it can be demonstrated that CCBC was successfully synthesized at temperatures of 500–700 °C. Although there is no difference in the crystalline structure, the porosity of the material (surface area, pore volume) is significantly influenced by the pyrolysis temperature.

3.2.3 FTIR analysis. FTIR spectrum (Fig. 2d) shows the changes in several characteristic vibrations of the CCBC samples synthesized at 500–700 °C. The most noticeable change is the loss or significant reduction of signals for several vibrations in the wavenumber range of 1600–1000 cm^{-1} as the pyrolysis temperature increases from 500 °C to 600 °C and 700 °C, respectively. Specifically, the characteristic vibrations for some functional groups of organic compounds on the suface of biochar at wavenumbers 1425 cm^{-1}, and 1379 cm^{-1} (C=O in COO$^-$) have completely disappeared or reduced in signal at pyrolysis temperatures of 600–700 °C.[41] The bands around 1580–1540 cm^{-1} was related to aromatic C=C, C=O stretching vibration modes of the carboxyl group, hydroxyl group and lactone.[42] The aromatic C=C stretching vibration (1460 cm^{-1}) also appeared in the FTIR spectrum with a weak signal. Especially, the characteristic vibrational modes of the C–O bond in obtuse angles also shift from higher wavenumbers (1163 cm^{-1} at 500 °C) to lower ones (1074 cm^{-1} at 600 °C and 1060 cm^{-1} at 700 °C).[43,44] According to studies, this vibration arises from the transformation of aromatic compounds in the form of alcohols, aldehydes, and carboxylic acids into compounds with C–O–C bonds in aromatic rings when pyrolyzed at high temperatures (700–800 °C).[45] The shift to lower wavenumbers suggests that

their chemical bonds are likely weaker, reducing the energy required to excite bond vibrations.[46] On the other hand, the vibration band at 1060–1163 cm^{-1} can also be attributed to the Si–O–Si group,[47,48] as silicon is commonly found in biomass and is an essential nutrient for corn growth.[30] However, the Si content in the corn core, as determined by the EDX method, is approximately 3.26%, which is significantly lower compared to the C content (88.83%). Therefore, we attribute the vibrations in the range of 1163–1060 cm^{-1} are C–O–C vibration.

In summary, pyrolysis conditions affect the properties and characteristics of biochar materials synthesized from corncobs. The degree of carbonization increases with the pyrolysis temperature, which also means that the surface area and pore volume of the material increase accordingly. However, retaining functional groups is necessary for adsorption in some cases.[49] This depends on the target pollutant and the adsorption mechanisms that may occur, allowing for the selection of appropriate pyrolysis conditions. In this study, CCBC is aimed at treating Cr(vi) in aqueous solutions. To select the material sample with the best adsorption efficiency, some preliminary surveys are necessary. Specifically, the Cr(vi) adsorption capacity under identical fixed conditions on 09 CCBC samples synthesized at 500 °C, 600 °C, and 700 °C for 15, 30, and 45 minutes was conducted.

3.3. Factors influencing Cr(vi) adsorption onto CCBC

3.3.1 Initial investigation. Studies have shown that pH is a major determinant in the adsorption capacity of Cr(vi). The optimal pH for Cr(vi) adsorption on biochar is generally 2.0.[48]

Therefore, Cr(VI) adsorption experiments at pH = 2.0 were conducted on 09 CCBC samples, and the results are presented in Table S4.† Additionally, the color of the 09 solutions after Cr(VI) adsorption is shown in Fig. S1.† Results indicate that the sample pyrolyzed at a higher temperature exhibits better Cr(VI) adsorption capacity. This initially suggests that Cr(VI) adsorption on CCBC may depend more on the porous structures and the functional groups on the material's surface (such as C–O–C, C=O, C=C, Si–O–Si). The changes in biochar structure lead to variations in porosity (Table S3†) and functional groups (Fig. 2d). Biochar synthesized at 700 °C has a significantly higher surface area and pore volume compared to those synthesized at 500–600 °C. Simultaneously, the functional groups (C–O–C/Si–O–Si), (C=C, C=O) exhibited shifts in their vibration to lower wavenumbers, specifically (1580–1540 cm^{-1}), and (1163–1060 cm^{-1}), indicating that they are more likely to participate in chemical processes to enhance adsorption capacity.[31] Additionally, it can be observed that the pyrolysis time of corncob has an insignificant effect on the % removal of Cr(VI) from aqueous solution. For instance, at a pyrolysis temperature of 500 °C for 15, 30, and 45 minutes, the % removal of Cr(VI) slightly increased to 31.2%, 32.5%, and 32.9%, respectively. This trend is similar for corncob samples pyrolyzed at 600 °C. For corncob samples pyrolyzed at 700 °C, the % removal of Cr(VI) slightly decreases with increasing pyrolysis time. However, according to Table S4,† this value is not significant (57.6%, 56.5%, and 55.3% for the 15, 30, and 45 minute samples, respectively). This may be due to the prolonged pyrolysis at high temperatures leading to greater decomposition

of functional groups capable of participating in Cr(VI) adsorption. Therefore, the CCBC sample synthesized at 700 °C for 15 minutes was selected to investigate the factors affecting the Cr(VI) adsorption process in aqueous solutions.

3.3.2 Effect of pH. The effect of pH on the adsorption of Cr(VI) on CCBC is presented in Fig. 3a and ANOVA analysis (ESI†). The p-value of 2.58×10^{-12} smaller than 0.05 indicated the significant impact of different pH on the Cr(VI) removal of Vietnamese corncob biochar. Specifically, CCBC exhibited the highest Cr(VI) adsorption efficiency at pH 2.0, with an efficiency of approximately 57.5% ($C_0 = 85$ mg L^{-1}). This pH value is consistent with the pH values reported by other authors.[48] It can be observed that the percentage of Cr(VI) removal gradually decreases with increasing pH values. Particularly in basic environments, the Cr(VI) adsorption capacity is significantly lower compared to acidic environments. This phenomenon can be explained based on the pH$_{PZC}$ value of CCBC presented in Fig. 3b (pH$_{PZC}$ = 7.6). When pH < pH$_{PZC}$, the surface of CCBC is positively charged, leading to effective adsorption of Cr(VI) anions through electrostatic interactions.[50] As the pH increases, the concentration of H$^+$ decreases, reducing the positive charge and consequently the adsorption capacity. When pH > pH$_{PZC}$, the surface of CCBC becomes negatively charged, which is not favorable for the adsorption of Cr(VI) anions through electrostatic interactions.[51] These results indicate that electrostatic interactions play a crucial role in the adsorption process of Cr(VI) on CCBC.

3.3.3 Effect of sorbent dosage. From the results of the pH effect survey, it was observed that the Cr(VI) removal efficiency
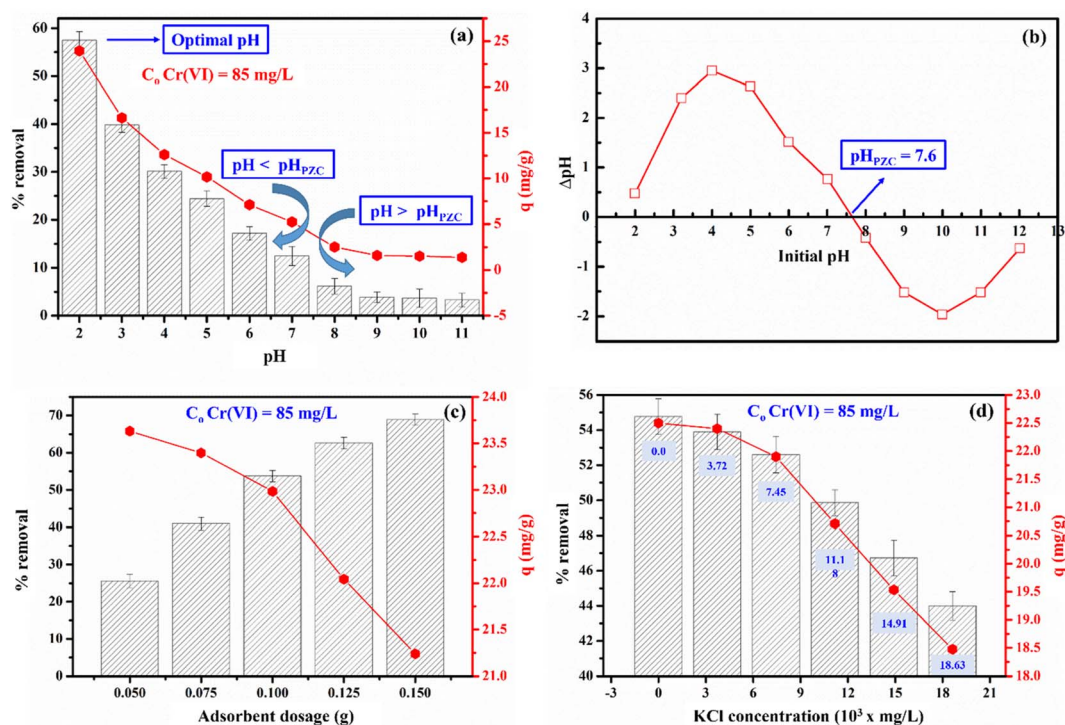

Fig. 3 The influence of pH on the adsorption of Cr(VI) onto CCBC (a); the isoelectric point of CCBC (b); adsorbent dosage (c) and ionic strength (d).

was only about 57% at an initial Cr(VI) concentration (C_0) of 85 mg L^{-1}. To enhance the treatment efficiency and evaluate the impact of CCBC mass on the Cr(VI) adsorption process, this study investigated the effect of CCBC mass (0.05–0.15 g) at an initial Cr(VI) concentration (C_0) of 85 mg L^{-1}. ANOVA: single factor analysis (ESI†) showed that the p-value of 3.45×10^{-16} smaller than 0.05 indicated the significant impact of different sorbent dosage on the Cr(VI) uptake of Vietnamese corncob biochar. In addition, the results presented in Fig. 3c indicate that % of Cr(VI) removal increases with the mass of the material. This can be explained by the fact that, as the mass of the material increases while keeping the solution volume constant (increasing m/V), a larger number of available adsorption sites can easily adsorb Cr(VI) from the solution, thereby enhancing the adsorption capacity. This result is consistent with several previously published studies.[16,52] Thus, the highest Cr(VI) removal efficiency reached approximately 70% with a CCBC mass of 0.15 g. However, since the removal percentage does not increase exponentially, the adsorption capacity, as calculated by eqn (2), decreases. Indeed, although the removal efficiency increased from 53% to 69% when the CCBC mass was increased from 0.10 g to 0.15 g, the adsorption capacity decreased from 26.5 mg g^{-1} to 21.2 mg g^{-1}.

3.3.4 Effect of ionic strength. In this study, KCl solution (3.72×10^3 to 18.63×10^3 mg L^{-1}) was selected to investigate the effect of competitive adsorption. The results presented in Fig. 3d clearly indicate competitive adsorption between Cr(VI) anions and Cl$^-$ ions, as the Cr(VI) removal efficiency decreased in the presence of KCl compared to its absence. However, different KCl concentrations did not significantly affect the Cr(VI) adsorption capacity due to the p-value calculated from ANOVA: single factor analysis to be 0.4 higher than 0.05 (ESI†). For instance, the Cr(VI) removal percentage slightly decreased from 54.77 to 53.89 and 52.60% when using low concentrations of KCl (3.72–7.45×10^3 mg L^{-1}). Nevertheless, at higher KCl concentrations (11.18–18.63×10^3 mg L^{-1}), the impact of competitive adsorption became more pronounced. Indeed, the Cr(VI) removal percentage further decreased to 49.86, 46.7, and 43.99% at KCl concentrations of 11.18, 14.91, and 18.63×10^3 mg L^{-1}, respectively. This phenomenon is explained by the competitive adsorption between Cl$^-$ anion and Cr$_2$O$_7^{2-}$/HCrO$_4^-$ at pH = 2.0. The Cl$^-$ anions occupy the adsorption sites on the surface of CCBC, and the competition increases with higher Cl$^-$ concentrations.[53] Consequently, the Cr(VI) adsorption capacity gradually decreases. This trend is similar to the Cr(VI) adsorption capacity on biochar derived from *Enteromorpha prolifera* and cotton wood.[48,54]

3.3.5 Desorption and recyclability. The desorption and reuse capabilities are crucial criteria when evaluating the potential application of materials in environmental remediation. Therefore, in this study, we conducted the desorption of Cr(VI) from CCBC using NaOH solutions at various concentrations to determine the optimal desorption conditions. Several previous studies have also employed NaOH to desorb anions from materials through anion exchange mechanisms.[48,55] The results of the survey on the effect of NaOH solution concentration on the desorption capacity of Cr(VI) from CCBC are

presented in Fig. S2a.† It can be observed that the higher the concentration of NaOH solution used, the better the desorption capacity of Cr(VI) due to easier anion exchange. For instance, the desorption efficiency of Cr(VI) is only about 17% at a NaOH concentration of 0.1 M. However, this value increased to approximately 42% when using 0.5 M NaOH. The best desorption capacity was achieved at a NaOH concentration of 0.9 M, with around 70%. If the NaOH concentration is further increased, the desorption capacity will continue to rise; however, this leads to chemical waste and environmental pollution. Therefore, we selected 0.9 M NaOH for subsequent investigations. Fig. S2b† illustrates the reusability of CCBC. Specifically, after 4 cycles of Cr(VI) adsorption–desorption at an initial Cr(VI) concentration of 85 mg L^{-1}, the Cr(VI) removal efficiency of CCBC decreased insignificantly and remained at approximately 63%. This indicates that CCBC can effectively adsorb Cr(VI) in aqueous solutions, demonstrating potential applications in environmental remediation.

3.4. Investigation of kinetic and isotherm on the Cr(VI) adsorption by CCBC

3.4.1 Influence of contact time on kinetic adsorption. ANOVA: single factor analysis showed the p-value to be 1.87×10^{-24} smaller than 0.05, confirming that the different contact time affected the Cr(VI) adsorption of Vietnamese corncob biochar (ESI†). This is also presented in Fig. 4a. It can be seen that within just 5 minutes, a significant amount of Cr(VI) was adsorbed onto CCBC (30%). The adsorption of Cr(VI) gradually increased and nearly reached adsorption equilibrium after 180 minutes. This can be explained by the strong interaction between Cr(VI) ions and the adsorption sites on the surface of CCBC during the first 180 minutes, leading to increased adsorption efficiency, especially in the first 5 minutes. After 180 minutes, the adsorption sites may become saturated with Cr(VI) ions, resulting in the adsorption efficiency remaining almost unchanged even though the adsorption time was extended to 270 minutes. Thus, it can be concluded that the adsorption process reaches equilibrium at 180 minutes with an adsorption efficiency of Cr(VI) reaching approximately 56%.

Additionally, to understand the nature of adsorption, the experimental data were analyzed using four kinetic models. The graphs of these models are presented in Fig. 4c, and the parameters calculated from their nonlinear equations are shown in Table 1. It can be seen that the Elovich kinetic model fits the experimental data best because it has the highest R^2 value (0.9752) and the lowest RMSE (0.4421) and χ^2 values (0.1281). The value of $\alpha = 791$, which is much greater than $\beta = 0.4669$, demonstrates that the adsorption process is predominantly chemical adsorption. In addition, the C value determined from the intraparticle diffusion kinetic model is different from 0 (16.0704), indicating that the adsorption of Cr(VI) by CCBC occurs through more than one mechanism.[56] In general, most adsorption processes change over time as $t^{1/2}$ rather than time t.[57] Therefore, the intraparticle diffusion equation was developed to describe the relationship between the amount of adsorbed substance (Q_e) and time $t^{1/2}$ (Fig. 4b).
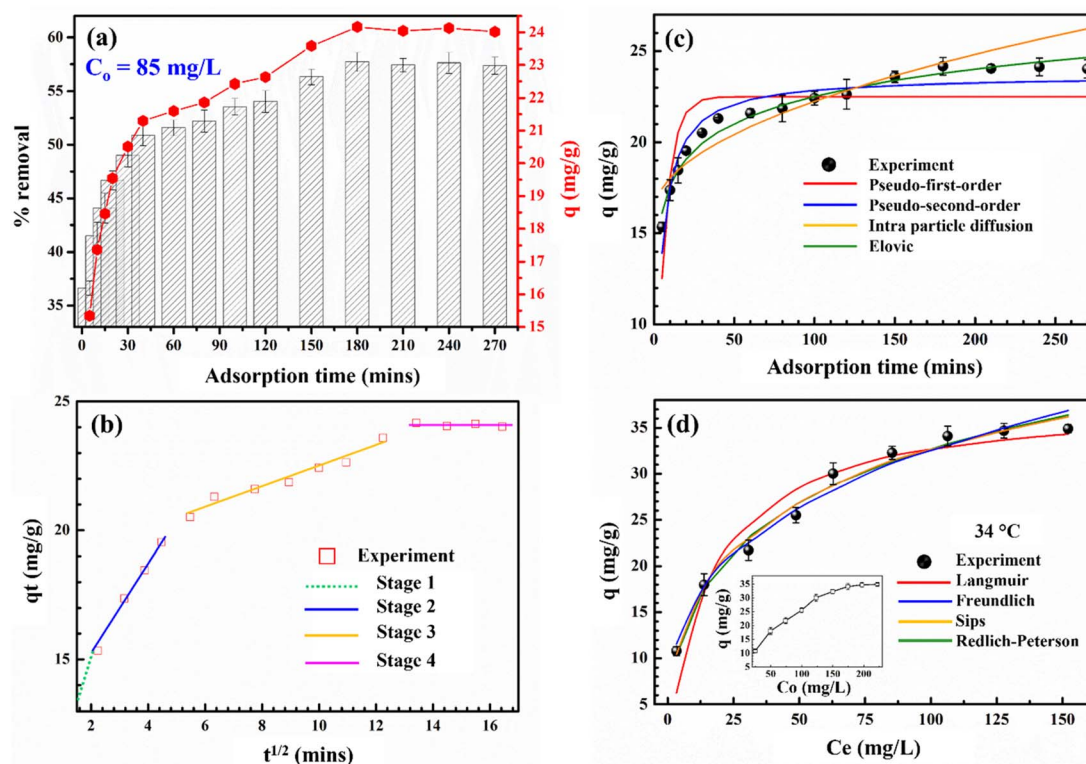
Fig. 4 Effect of adsorption time (a); plots of $t^{1/2}-q_t$ (b); plots of kinetic models (c); and plots isotherm models (d) of the Cr(VI) adsorption onto CCBC.

Table 1 The parameters of kinetic models for the adsorption of Cr(VI) onto CCBC

Types of models	Parameters	Values
Experiment	C_0 (mg L^{-1})	83.76
	$q_{e(exp)}$ (mg g^{-1})	24.17
Pseudo-first-order	$q_{e(cal)}$ (mg g^{-1})	22.51
	k_1 (min^{-1})	0.16
	RMSE	1.69
	R^2	0.66
	χ^2	1.76
Pseudo-second-order	$q_{e(cal)}$ (mg g^{-1})	23.66
	k_2 (g mg^{-1} min^{-1})	0.01
	RMSE	0.81
	R^2	0.92
	χ^2	0.40
Intraparticle diffusion	K_d	0.62
	C	16.07
	RMSE	0.74
	R^2	0.89
	χ^2	0.55
Elovic	α (mg g^{-1} min^{-1})	791
	β (mg g^{-1})	0.47
	RMSE	0.44
	R^2	0.98
	χ^2	0.13

The adsorption of heavy metals typically occurs in four stages:[58] bulk diffusion (1); surface diffusion (2); intraparticle diffusion (3); and adsorption equilibrium (4). Accordingly, the adsorption of Cr(VI) on CCBC can occur in four stages. In stage 1 (green line), adsorption occurs very rapidly through mass transfer; in stage 2 (blue line), rapid adsorption of Cr(VI) continues due to the abundance of adsorption sites on the material's surface; in stage 3 (orange line), gradual adsorption continues, and this stage is crucial for adsorption kinetics; in stage 4 (pink line), adsorption reaches equilibrium as most of the adsorption sites become occupied.[59]

3.4.2 The study of isotherm adsorption models. The isotherm models for the adsorption of Cr(VI) on CCBC are presented in Fig. 4d, and the parameters of these models are listed in Table S5.† The results indicate that the experimental data is best described by the Sips isotherm model, as it has the highest R^2 value (0.9845) and the lowest RMSE (1.0638) and χ^2 values (0.3318). This suggests that the adsorption process involves both monolayer and multilayer adsorption. From Fig. 4d, it can be observed that as the initial concentration of the Cr(VI) solution increases, the adsorption capacity of Cr(VI) rapidly rises and gradually reaches equilibrium at higher concentration values. This phenomenon can be explained by the progressive occupation of adsorption sites on the surface of CCBC until these sites are fully occupied.[48] Table 2 compares the Cr(VI) adsorption capacity with other materials. It can be observed that the maximum Cr(VI) adsorption capacity (Q_m) of CCBC in this study is significantly higher than that of biochar synthesized from various by-products such as Durian shells,[27] Oak wood.[28] Additionally, compared to activated carbon, composites, and magnetic biochar material-based corncob biomass, the Cr(VI)

Table 2 Comparison the Cr(VI) adsorption capacity of biochar with other materials

Materials	Sources	Q_m (mg g^{-1})	References
Biochar	Corncob	38.13	This study
	Durian shells	6.66	27
	Oak wood	3.03	28
	Pine sawdust	21.03	60
Activated carbon	Corncob	9.90	21
	Corncob	25.69	22
	Slurry	38.17	61
Composite	Corncob activated carbon + banana peel	35.84	62
	Biochar + bentonite + rarasaponin	23.02	27
	MnO$_2$ + chitosan	61.56	55
Magnetic biochar	Fe$_2$O$_3$/corncob biochar	25.94	24
	Polypyrrol/corncob	19.23	25
	Phoenix tree leaves + nano Fe$_3$O$_4$	19.02	63
	Waste reed + nano Fe$_3$O$_4$	9.92	64

adsorption capacity is also higher. For instance, G. K. Gupta *et al.* modified CCBC using phosphoric acid and adsorbed Cr(VI), achieving a Q_m of 25.69 mg g^{-1}, which is lower than our result (38.13 mg g^{-1}).[22] The adsorption capacities decrease in the following order: biochar (38.13 mg g^{-1}) > composite (35.84 mg g^{-1}) > activated carbon (25.69 mg g^{-1}) > magnetic biochar (19.23 mg g^{-1}). Overall, the biochar synthesized from corncob in this study demonstrates considerable potential for application in the treatment of Cr(VI) in aqueous solutions.

3.5. Proposed mechanism of Cr(VI) adsorption onto CCBC

The adsorption of Cr(VI) onto biochar can follow chemical or physical processes *via* several mechanisms such as electrostatic interactions,[55] ion exchange,[24] surface complexation,[65] combined reduction–adsorption,[65] and pore diffusion.[66] These adsorption mechanisms are demonstrated through a combination of theoretical model studies (kinetics, isotherms); chemical–physical methods such as XRD, BET-BJH, SEM-EDX, XPS, FTIR, TGA-DSC; XANES, confocal μ-XRF mapping; and physical methods such as positron annihilation lifetime (PAL) and electron momentum (EMD) measurements.[67,68] In this study, chemical–physical methods including BET, FTIR, SEM, EDX, and XRD were used to investigate the mechanisms of Cr(VI) adsorption onto CCBC.

3.5.1 BET analysis. Fig. 5 presents the N$_2$ adsorption–desorption isotherms at −196 °C and FTIR spectra of CCBC before and after Cr(VI) adsorption. From Fig. 5a, it can be observed that the isotherms of the material before and after Cr(VI) adsorption are both classified as type IV according to IUPAC classification, due to the hysteresis in the relative pressure region P/P_0 around 0.5. However, the amount of adsorbed N$_2$ significantly decreased, corresponding to a reduction in the surface area of the material. Specifically, the surface area of the material decreased from 443 m^2 g^{-1} to 382 m^2 g^{-1}. Notably, the external surface area values changed very little, with values of 27 m^2 g^{-1} and 24 m^2 g^{-1} for the material before and after adsorption, respectively. In contrast, the internal surface area significantly decreased from 416 m^2 g^{-1} to 358 m^2 g^{-1}. This demonstrates that the Cr(VI) adsorption process primarily occurs on the internal surface. In other words, the adsorption of Cr(VI) on CCBC may proceed *via* a pore diffusion mechanism. These results indicate that surface area plays a crucial role in the adsorption of Cr(VI) on CCBC. Similar to our previous study on the adsorption of Pb(II) on ZSM-5 zeolite, a similar trend has been confirmed by BET results.[52]

3.5.2 FTIR analysis. Fig. 5b presents the FTIR spectra of CCBC before and after Cr(VI) adsorption. After adsorption, several functional groups and characteristic vibrations remain
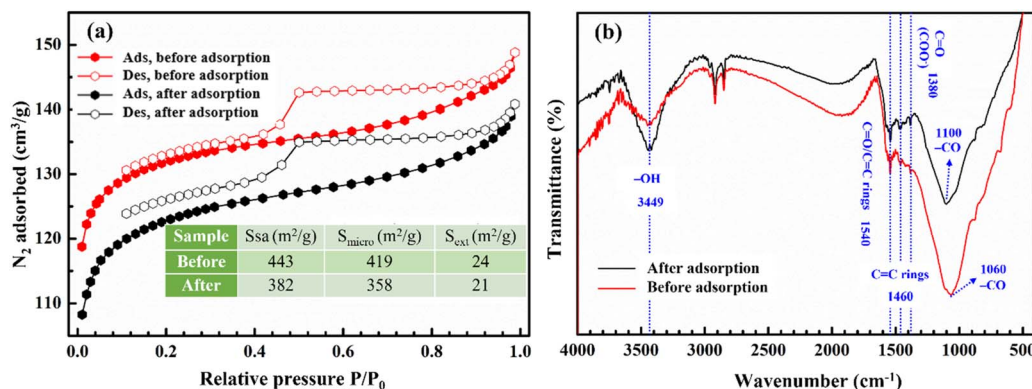

Fig. 5 N$_2$ adsorption–desorption at 77 K (a); FTIR spectra (b) of CCBC before and after Cr(VI) adsorption.

unchanged. For instance; C=C rings (1540 cm^{-1}); and C=O in COOH (1380 cm^{-1}) retain their positions and peak shapes. Meanwhile, the characteristic vibration of the –OH group, although unchanged in wavenumber at the peak (3449 cm^{-1}), becomes sharper and increases in transmittance after adsorption. The characteristic vibration for the C–O bond in the aromatic ring shifts from 1060 cm^{-1} to 1100 cm^{-1} and significantly decreases in transmittance.[43] Additionally, the aromatic C=C vibration (1460 cm^{-1}) becomes more pronounced after adsorption. This suggests that Cr(VI) adsorption may involve OH, C–O–C, and C=C functional groups and follow by chemical process. These results are consistent with kinetic studies. The experimental data best fit the Elovich kinetic model, and the significantly higher value of α compared to β indicates that the adsorption occurs via a chemical mechanism. Some studies indicate that at pH = 2.0, $HCrO_4^-$/$Cr_2O_7^{2-}$ can be reduced to Cr^{3+} due to their strong oxidizing nature at this pH.[69] Therefore, adsorption mechanism that may occur on CCBC is the formation of surface complexes between Cr^{3+} cation and aromatic C=C rings (C_π–cation)[66] or cation exchange. In this study, we demonstrate this mechanism through the combination of FTIR and EDX spectra analysis.

3.5.3 SEM-EDX analysis. The SEM and EDX analysis results of CCBC before and after Cr(VI) adsorption are presented in Fig. 6. As shown in Fig. 6a, the surface of CCBC is rough, featuring numerous grooves, channels, and large pores with diameters around 10 μm, as well as smaller pores approximately 1 μm in diameter. These sites are suitable for Cr(VI) adsorption. The SEM images indicate that after adsorption, the surface morphology of the material remains largely unchanged,

retaining the pores and grooves (Fig. 6b). The combination of XRD patterns (Fig. S2a†) and SEM images (Fig. S2b†) of the material after four reuse cycles demonstrates the high durability of CCBC. The EDX spectrum of the material reveals significant changes in the chemical elemental composition between the pre-adsorption (Fig. 6c) and post-adsorption (Fig. 6d) samples of Cr(VI). Specifically, the presence of Cr and the disappearance of K and Si elements in the post-adsorption sample indicate that Cr adsorption likely occurred through an ion exchange mechanism involving K^+, Si^{4+}, and Cr^{3+}. This finding further suggests the adsorption of Cr(VI) onto the surface of biochar and the reduction of Cr(VI) to Cr(III), with the Cr(III) ions interacting with the biochar via two mechanisms: surface complexation and ion exchange. After adsorption, besides the loss of K, Si was also no longer present in the CCBC sample, which suggests the possibility of ion exchange between Si^{4+} and Cr^{3+}. Studies have indicated that in biochar, Si exists in the form of amorphous hydrated silica, i.e., $SiO_2 \cdot nH_2O$[30,31] and the surface often contains silanol groups (Si–OH).[70] Therefore, two key adsorption mechanisms in this study are surface adsorption (Cr(VI)-biochar) followed by the reduction of Cr(VI) to Cr(III), allowing ion exchange adsorption to occur. The EDX spectrum also reveals that, in addition to C and O, the composition of CCBC in this study includes several other elements such as K, Si, and P, similar to previously published research.[71] This indicates that the origin of the corncob might be the cause of the differences in chemical composition, as they are related to the variety, growth, and development conditions of the corn. Furthermore, a recent study on the Cr(VI) removal capability through bioreduction using corncob also
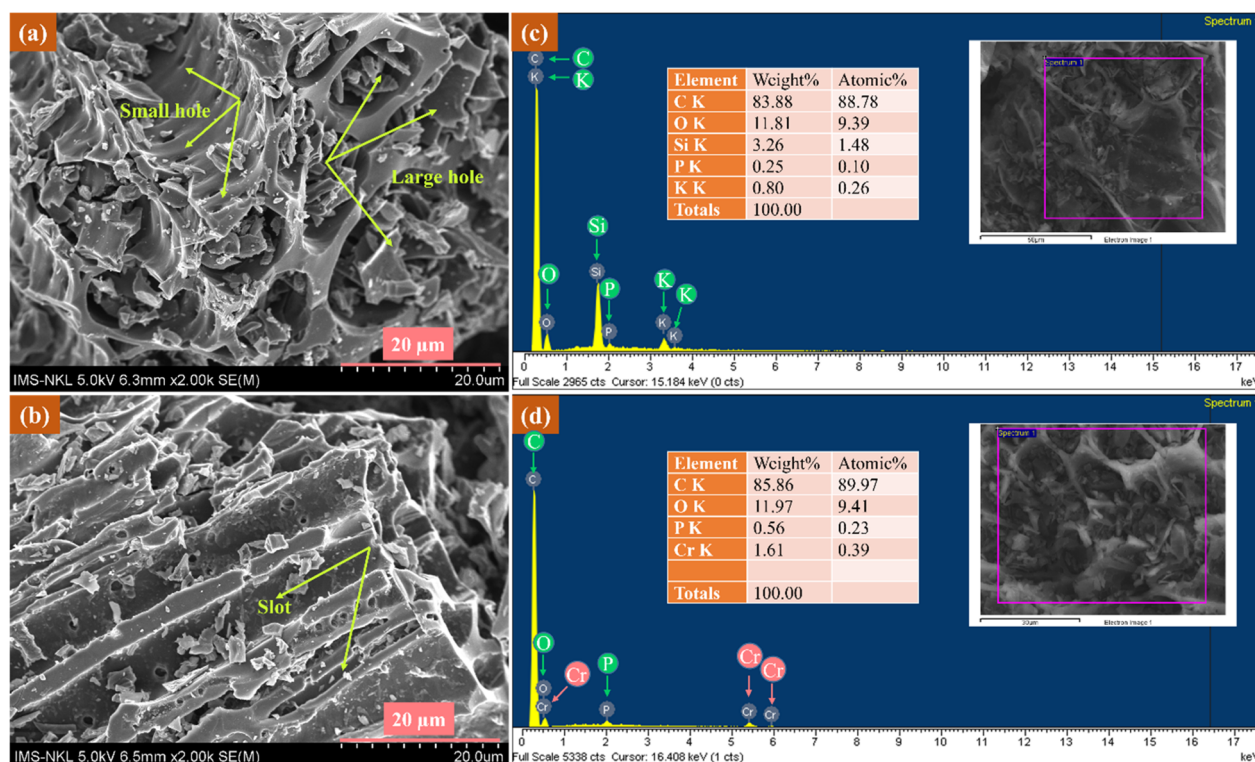

Fig. 6 SEM image (a and b); EDX spectra (c and d) of CCBC before and after Cr(VI) adsorption.
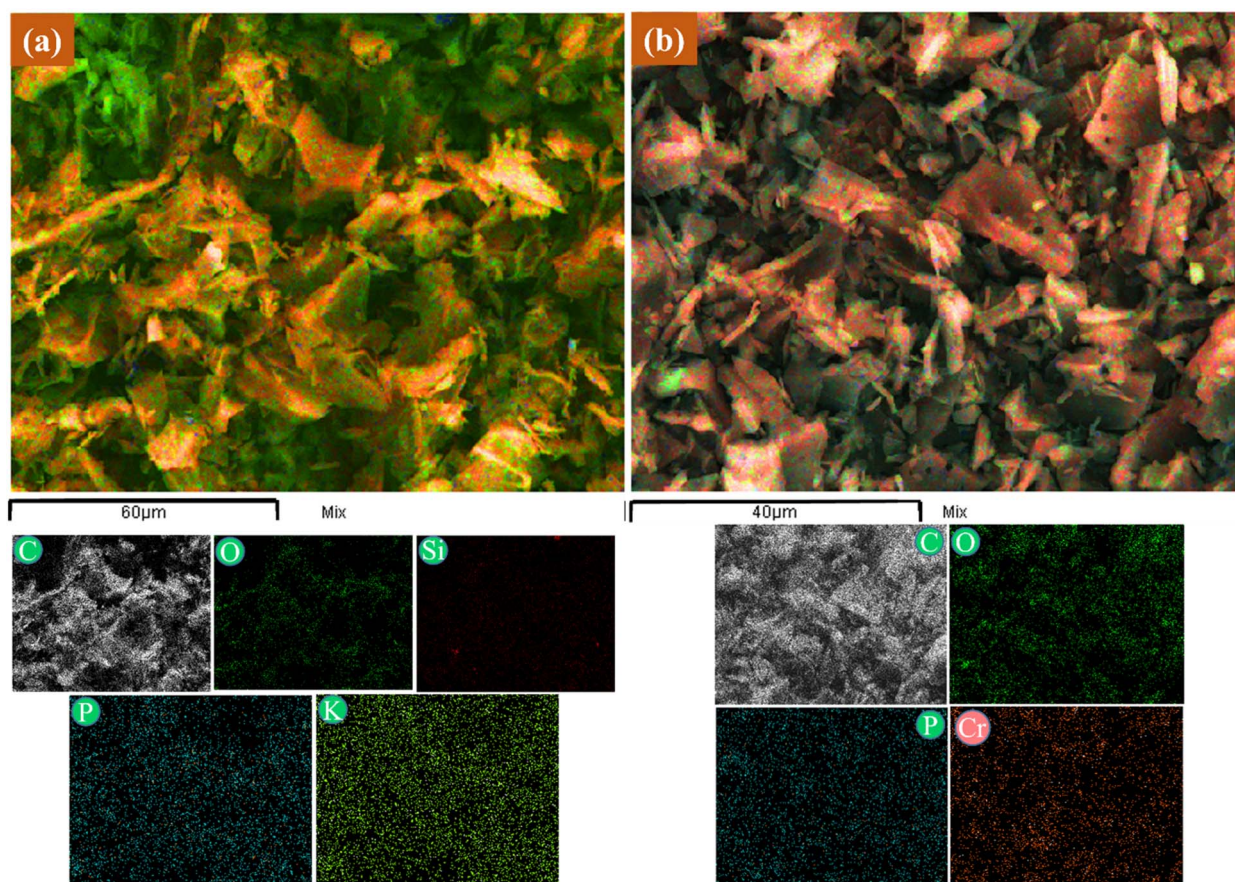
Fig. 7 SEM-mapping of CCBC before (a) and after (b) Cr(VI) adsorption.

demonstrated that corncob can reduce Cr(VI) to Cr(III). This process occurs through several primary mechanisms including: carrier effect, nutrient element release and electron shuttle.[72]

3.5.4 SEM-mapping analysis. The SEM-mapping images of CCBC before and after Cr(VI) adsorption are presented in Fig. 7. It can be observed that after adsorption, elements such as K and Si are no longer present, while Cr appears. Notably, Cr is uniformly distributed across the entire surface of the biochar material (red regions in the map (Fig. 7b)). Thus, combining SEM-EDX and SEM-mapping results has demonstrated that Cr(VI) adsorption onto CCBC primarily occurs through electrostatic interactions and cation exchange compared to other mechanisms. This result is consistent with previous publications by several authors.[73–75] In summary, Cr(VI) adsorption in aqueous solution on CCBC material can occur through several proposed mechanisms shown in Fig. S4,† including pore diffusion, electrostatic interaction, ion exchange, and surface complexation.

4. Conclusion

In this study, CCBC was successfully synthesized *via* pyrolysis, with the optimal pyrolysis conditions for Cr(VI) adsorption being 700 °C for 15 minutes. The surface area of CCBC significantly increased from 6.7 to 443 $m^2 g^{-1}$ (66 times) while the functional groups characteristic on the surface of biochar changed as the pyrolysis temperature increased from 500 to 700 °C. The maximum Cr(VI) adsorption capacity according to the Langmuir model reached 38.13 mg g^{-1}, which is higher compared to previously reported corncob-based materials such as activated carbon, composites, and magnetic biochar. Based on physico-chemical analysis methods, the adsorption of Cr(VI) on CCBC occurs through two main mechanisms composed of reduction and ion exchange. Cr(VI) can be effectively desorbed using NaOH and subsequently reused. However, the use of high concentrations of NaOH should be carefully considered to avoid negative environmental impacts. For practical applications, the material can be fabricated into porous composite granules and used in dynamic adsorption processes. The material can be easily recovered and processed after use, either for reuse or disposal.

Data availability

The datasets generated and/or analyzed during the current study are available from the corresponding author on reasonable request. The data include experimental results on the effects of pH, adsorption time, initial Cr(VI) concentration, material mass, and ionic strength on the adsorption process, as well as kinetic and isotherm models for Cr(VI) adsorption. Additionally, FTIR spectra and SEM-EDX analysis data used to investigate the functional groups and surface morphology of the biochar are included.

Conflicts of interest

Acknowledgements

References

1 H. R. Mian, S. Haydar and G. Hussain, Optimization of sequencing batch reactor for wastewater treatment using chemically enhanced primary treatment as a pre-treatment, *Water SA*, 2018, **44**, 399–405.

2 B. Dhanalakshmi and G. Gawdaman, Determination of heavy metals in goat milk through ICP-OES, *Asian J. Dairy Food Res.*, 2013, **32**, 186–190.

3 M. Mondal, Removal of Pb (II) from industrial wastewater by using various natural materials–a review, *Int. J. Sustain. Dev. Plann.*, 2008, **3**, 377–393.

4 R. L. Canfield, C. R. Henderson, D. A. Cory-Slechta, C. Cox, T. A. Jusko and B. P. Lanphear, Intellectual Impairment in Children with Blood Lead Concentrations below 10 μg per Deciliter, *N. Engl. J. Med.*, 2003, **348**, 1517–1526.

5 D. M. Proctor, M. Suh, L. Mittal, S. Hirsch, R. Valdes Salgado, C. Bartlett, C. Van Landingham, A. Rohr and K. Crump, Inhalation cancer risk assessment of hexavalent chromium based on updated mortality for Painesville chromate production workers, *J. Exposure Sci. Environ. Epidemiol.*, 2016, **26**, 224–231.

6 N. P. Raval, P. U. Shah and N. K. Shah, Adsorptive removal of nickel(II) ions from aqueous environment: A review, *J. Environ. Manage.*, 2016, **179**, 1–20.

7 M. A. Acheampong, J. P. C. Pereira, R. J. W. Meulepas and P. N. L. Lens, Kinetics modelling of Cu(II) biosorption on to coconut shell and Moringa oleifera seeds from tropical regions, *Environ. Technol.*, 2012, **33**, 409–417.

8 M. Gheju, I. Balcu and G. Mosoarca, Removal of Cr(VI) from aqueous solutions by adsorption on MnO2, *J. Hazard. Mater.*, 2016, **310**, 270–277.

9 X.-Z. Wei, Z.-Q. Gan, Y.-J. Shen, Z.-L. Qiu, L.-F. Fang and B.-K. Zhu, Negatively-charged nanofiltration membrane and its hexavalent chromium removal performance, *J. Colloid Interface Sci.*, 2019, **553**, 475–483.

10 E. Abbasi-Garravand and C. N. Mulligan, Using micellar enhanced ultrafiltration and reduction techniques for removal of Cr(VI) and Cr(III) from water, *Sep. Purif. Technol.*, 2014, **132**, 505–512.

11 Z. Pan, X. Zhu, A. Satpathy, W. Li, J. D. Fortner and D. E. Giammar, Cr(VI) Adsorption on Engineered Iron Oxide Nanoparticles: Exploring Complexation Processes and Water Chemistry, *Environ. Sci. Technol.*, 2019, **53**, 11913–11921.

12 J. El Gaayda, Y. Rachid, F. E. Titchou, I. Barra, A. Hsini, P.-S. Yap, W.-D. Oh, C. Swanson, M. Hamdani and R. A. Akbour, Optimizing removal of chromium (VI) ions from water by coagulation process using central composite design: Effectiveness of grape seed as a green coagulant, *Sep. Purif. Technol.*, 2023, **307**, 122805.

13 H. Yin, Q. Guo, C. Lei, W. Chen and B. Huang, Electrochemical-driven carbocatalysis as highly efficient advanced oxidation processes for simultaneous removal of humic acid and Cr(VI), *Chem. Eng. J.*, 2020, **396**, 125156.

14 Q. Jina, W. Yaob and X. Chenc, Removal of Cr (VI) from wastewater by simplified electrodeionization, *Desalin. Water Treat.*, 2020, **183**, 301–306.

15 Y. Ren, Y. Han, X. Lei, C. Lu, J. Liu, G. Zhang, B. Zhang and Q. Zhang, A magnetic ion exchange resin with high efficiency of removing Cr (VI), *Colloids Surf., A*, 2020, **604**, 125279.

16 V.-P. Dinh, D.-K. Nguyen, T.-T. Luu, Q.-H. Nguyen, L. A. Tuyen, D. D. Phong, H. A. T. Kiet, T.-H. Ho, T. T. P. Nguyen, T. D. Xuan, P. T. Hue and N. T. N. Hue, Adsorption of Pb(II) from aqueous solution by pomelo fruit peel-derived biochar, *Mater. Chem. Phys.*, 2022, **285**, 126105.

17 P. T. Huynh, D.-K. Nguyen, B.-N. Duong, P.-H. Nguyen, P. N. T. Hong and V.-P. Dinh, Thermally treated biomass of pine (Pinus kesiya) leaves for effective removal of organic dyes from aqueous solutions, *J. Chem. Technol. Biotechnol.*, 2024, **99**, 307–316.

18 T. Thuy-Nham Nguyen, A.-T. Hoang, D.-K. Nguyen, N.-A. Nguyen and V.-P. Dinh, Initial study of the column adsorption of radioactive iodine onto mixture of composite material ZSM-5/PVA and biochar/PVA, *J. Clin. Pharm.*, 2023, **18**, 186–192.

19 G. Enaime, A. Baçaoui, A. Yaacoubi and M. Lübken, Biochar for Wastewater Treatment—Conversion Technologies and Applications, *Appl. Sci.*, 2020, **10**, 3492.

20 S. F. Billa, T. E. Angwafo and A. F. Ngome, Agro-environmental characterization of biochar issued from crop wastes in the humid forest zone of Cameroon, *Int. J. Recycl. Org. Waste Agric.*, 2019, **8**, 1–13.

21 H. Li, P. Gao, J. Cui, F. Zhang, F. Wang and J. Cheng, Preparation and Cr(VI) removal performance of corncob activated carbon, *Environ. Sci. Pollut. Res.*, 2018, **25**, 20743–20755.

22 G. K. Gupta, M. Ram, R. Bala, M. Kapur and M. K. Mondal, Pyrolysis of chemically treated corncob for biochar production and its application in Cr(VI) removal, *Environ. Prog. Sustain. Energy*, 2018, **37**, 1606–1617.

23 O. Xin, H. Yitong, C. Xi and C. Jiawei, Magnetic biochar combining adsorption and separation recycle for removal of chromium in aqueous solution, *Water Sci. Technol.*, 2016, **75**, 1177–1184.

24 L. P. Hoang, H. T. Van, L. H. Nguyen, D.-H. Mac, T. T. Vu, L. T. Ha and X. C. Nguyen, Removal of Cr(VI) from aqueous solution using magnetic modified biochar derived from raw corncob, *New J. Chem.*, 2019, **43**, 18663–18672.

25 Y. Yang, N. Chen, C. Feng, M. Li and Y. Gao, Chromium removal using a magnetic corncob biochar/polypyrrole composite by adsorption combined with reduction: reaction pathway and contribution degree, *Colloids Surf. A Physicochem. Eng. Asp.*, 2018, **556**, 201–209.

26 A. Shakya and T. Agarwal, Effect of pyrolysis temperature on physicochemical properties and hexavalent chromium adsorption of the corncob biochars, *Biomass Convers. Biorefin.*, 2023, **13**, 15197–15210.

27 L. Laysandra, F. H. Santosa, V. Austen, F. E. Soetaredjo, K. Foe, J. N. Putro, Y.-H. Ju and S. Ismadji, Rarasaponin-bentonite-activated biochar from durian shells composite for removal of crystal violet and Cr(VI) from aqueous solution, *Environ. Sci. Pollut. Res.*, 2018, **25**, 30680–30695.

28 D. Mohan, S. Rajput, V. K. Singh, P. H. Steele and C. U. Pittman, Modeling and evaluation of chromium remediation from water using low cost bio-char, a green adsorbent, *J. Hazard. Mater.*, 2011, **188**, 319–333.

29 A. H. M. G. Hyder, S. A. Begum and N. O. Egiebor, Adsorption isotherm and kinetic studies of hexavalent chromium removal from aqueous solution onto bone char, *J. Environ. Chem. Eng.*, 2015, **3**, 1329–1336.

30 Y. Wang, X. Xiao, Y. Xu and B. Chen, Environmental Effects of Silicon within Biochar (Sichar) and Carbon–Silicon Coupling Mechanisms: A Critical Review, *Environ. Sci. Technol.*, 2019, **53**, 13570–13582.

31 L. Qian, S. Liu, W. Zhang, Y. Chen, D. Ouyang, L. Han, J. Yan and M. Chen, Enhanced reduction and adsorption of hexavalent chromium by palladium and silicon rich biochar supported nanoscale zero-valent iron, *J. Colloid Interface Sci.*, 2019, **533**, 428–436.

32 X. Jin, M.-Q. Jiang, X.-Q. Shan, Z.-G. Pei, Z. Chen and I. Science, Adsorption of methylene blue and orange II onto unmodified and surfactant-modified zeolite, *J. Colloid Sci.*, 2008, **328**, 243–247.

33 V.-P. Dinh, N.-C. Le, L. A. Tuyen, N. Q. Hung, V.-D. Nguyen and N.-T. Nguyen, Insight into adsorption mechanism of lead(II) from aqueous solution by chitosan loaded MnO₂ nanoparticles, *Mater. Chem. Phys.*, 2018, **207**, 294–302.

34 K. Anupam, A. K. Sharma, P. S. Lal, S. Dutta and S. Maity, Preparation, characterization and optimization for upgrading Leucaena leucocephala bark to biochar fuel with high energy yielding, *Energy*, 2016, **106**, 743–756.

35 P. Basu, in *Biomass Gasification, Pyrolysis and Torrefaction*, ed. P. Basu, Academic Press, 3rd edn, 2018, pp. 155–187, DOI: 10.1016/B978-0-12-812992-0.00005-4.

36 Q. Sun, N. Wang, G. Guo, X. Chen and J. Yu, Synthesis of tri-level hierarchical SAPO-34 zeolite with intracrystalline micro–meso–macroporosity showing superior MTO performance, *J. Mater. Chem. A*, 2015, **3**, 19783–19789.

37 Y. Li, H. Shang, Y. Cao, C. Yang, Y. Feng and Y. Yu, High performance removal of sulfamethoxazole using large specific area of biochar derived from corncob xylose residue, *Biochar*, 2022, **4**, 11.

38 S. Wijitkosum and T. Sriburi, Applying Cassava Stems Biochar Produced from Agronomical Waste to Enhance the Yield and Productivity of Maize in Unfertile Soil, *Fermentation*, 2021, **7**, 277.

39 K. Saini, B. Biswas, A. Kumar, A. Sahoo, J. Kumar and T. Bhaskar, Screening of sugarcane bagasse-derived biochar for phenol adsorption: optimization study using response surface methodology, *Int. J. Environ. Sci. Technol.*, 2022, **19**, 8797–8810.

40 A. P. da Luz Corrêa, R. R. C. Bastos, G. N. d. Rocha Filho, J. R. Zamian and L. R. V. d. Conceição, Preparation of sulfonated carbon-based catalysts from murumuru kernel shell and their performance in the esterification reaction, *RSC Adv.*, 2020, **10**, 20245–20256.

41 C. Pituello, O. Francioso, G. Simonetti, A. Pisi, A. Torreggiani, A. Berti and F. Morari, Characterization of chemical–physical, structural and morphological properties of biochars from biowastes produced at different temperatures, *J. Soils Sediments*, 2015, **15**, 792–804.

42 P. Sun, C. Hui, R. Azim Khan, J. Du, Q. Zhang and Y.-H. Zhao, Efficient removal of crystal violet using Fe₃O₄-coated biochar: the role of the Fe₃O₄ nanoparticles and modeling study their adsorption behavior, *Sci. Rep.*, 2015, **5**, 12638.

43 L. Zhao, H. Zhang, B. Zhao and H. Lyu, Activation of peroxydisulfate by ball-milled α-FeOOH/biochar composite for phenol removal: Component contribution and internal mechanisms, *Environ. Pollut.*, 2022, **293**, 118596.

44 Q. An, X.-Q. Li, H.-Y. Nan, Y. Yu and J.-N. Jiang, The potential adsorption mechanism of the biochars with different modification processes to Cr(VI), *Environ. Sci. Pollut. Res.*, 2018, **25**, 31346–31357.

45 Z. Xu, X. Xu, Y. Zhang, Y. Yu and X. Cao, Pyrolysis-temperature depended electron donating and mediating mechanisms of biochar for Cr(VI) reduction, *J. Hazard. Mater.*, 2020, **388**, 121794.

46 A. Ricci, K. J. Olejar, G. P. Parpinello, P. A. Kilmartin and A. Versari, Application of Fourier Transform Infrared (FTIR) Spectroscopy in the Characterization of Tannins, *Appl. Spectrosc. Rev.*, 2015, **50**, 407–442.

47 L. Qian, X. Shang, B. Zhang, W. Zhang, A. Su, Y. Chen, D. Ouyang, L. Han, J. Yan and M. Chen, Enhanced removal of Cr(VI) by silicon rich biochar-supported nanoscale zero-valent iron, *Chemosphere*, 2019, **215**, 739–745.

48 Y. Chen, B. Wang, J. Xin, P. Sun and D. Wu, Adsorption behavior and mechanism of Cr(VI) by modified biochar derived from Enteromorpha prolifera, *Ecotoxicol. Environ. Saf.*, 2018, **164**, 440–447.

49 M. A. H. Badsha, M. Khan, B. Wu, A. Kumar and I. M. C. Lo, Role of surface functional groups of hydrogels in metal adsorption: From performance to mechanism, *J. Hazard. Mater.*, 2021, **408**, 124463.

50 Q. Zhang, Y. Li, Q. Yang, H. Chen, X. Chen, T. Jiao and Q. Peng, Distinguished Cr(VI) capture with rapid and superior capability using polydopamine microsphere: Behavior and mechanism, *J. Hazard. Mater.*, 2018, **342**, 732–740.

51 J. Fito, S. Tibebu and T. T. I. Nkambule, Optimization of Cr (VI) removal from aqueous solution with activated carbon derived from Eichhornia crassipes under response surface methodology, *BMC Chem.*, 2023, **17**, 4.

52 N.-A. Nguyen, D.-K. Nguyen, V.-P. Dinh, B.-N. Duong, L. Ton-That, N. T. Hung and T.-H. Ho, Effective adsorption of Pb(II) ion from aqueous solution onto ZSM-5 zeolite synthesized

from Vietnamese bentonite clay, *Environ. Monit. Assess.*, 2023, **195**, 1530.

53 J. Wang, X. Yin, W. Tang and H. Ma, Combined adsorption and reduction of Cr(VI) from aqueous solution on polyaniline/multiwalled carbon nanotubes composite, *Korean J. Chem. Eng.*, 2015, **32**, 1889–1895.

54 M. Zhang, B. Gao, S. Varnoosfaderani, A. Hebard, Y. Yao and M. Inyang, Preparation and characterization of a novel magnetic biochar for arsenic removal, *Bioresour. Technol.*, 2013, **130**, 457–462.

55 V.-P. Dinh, M.-D. Nguyen, Q. H. Nguyen, T.-T.-T. Do, T.-T. Luu, A. T. Luu, T. D. Tap, T.-H. Ho, T. P. Phan, T. D. Nguyen and L. V. Tan, Chitosan-MnO$_2$ nanocomposite for effective removal of Cr (VI) from aqueous solution, *Chemosphere*, 2020, **257**, 127147.

56 K.-J. Hwang, W.-G. Shim, Y. Kim, G. Kim, C. Choi, S. O. Kang and D. W. Cho, Dye adsorption mechanisms in TiO$_2$ films, and their effects on the photodynamic and photovoltaic properties in dye-sensitized solar cells, *Phys. Chem. Chem. Phys.*, 2015, **17**, 21974–21981.

57 W.-C. Tsai, S. Ibarra-Buscano, C.-C. Kan, C. M. Futalan, M. L. P. Dalida and M.-W. Wan, Removal of copper, nickel, lead, and zinc using chitosan-coated montmorillonite beads in single- and multi-metal system, *Desalin. Water Treat.*, 2016, **57**, 9799–9812.

58 M. E. Argun, S. Dursun, C. Ozdemir and M. Karatas, Heavy metal adsorption by modified oak sawdust: thermodynamics and kinetics, *J. Hazard. Mater.*, 2007, **141**, 77–85.

59 V.-P. Dinh, T.-D.-T. Huynh, H. M. Le, V.-D. Nguyen, V.-A. Dao, N. Q. Hung, L. A. Tuyen, S. Lee, J. Yi, T. D. Nguyen and L. V. Tan, Insight into the adsorption mechanisms of methylene blue and chromium(III) from aqueous solution onto pomelo fruit peel, *RSC Adv.*, 2019, **9**, 25847–25860.

60 X. Qin, R. Tao, S. Cheng, B. Xing, W. Meng, Y. Nie, C. Zhang and J. Yu, Microwave-assisted one-pot method preparation of ZnO decorated biochar for levofloxacin and Cr(VI) removal from wastewater, *Ind. Crops Prod.*, 2024, **208**, 117863.

61 V. K. Gupta, A. Rastogi and A. Nayak, Adsorption studies on the removal of hexavalent chromium from aqueous solution using a low cost fertilizer industry waste material, *J. Colloid Interface Sci.*, 2010, **342**, 135–141.

62 H. A. Areti, A. Jabesa, B. J. Daba and D. Jibril, Response surface method based parametric optimization of Cr(VI) removal from tannery wastewater using a mixed banana peel and corn cob activated carbon: Kinetic and isotherm modeling studies, *J. Water Proc. Eng.*, 2024, **59**, 104977.

63 S. Liang, S. Shi, H. Zhang, J. Qiu, W. Yu, M. Li, Q. Gan, W. Yu, K. Xiao, B. Liu, J. Hu, H. Hou and J. Yang, One-pot solvothermal synthesis of magnetic biochar from waste biomass: Formation mechanism and efficient adsorption of Cr(VI) in an aqueous solution, *Sci. Total Environ.*, 2019, **695**, 133886.

64 X. Song, Y. Zhang, N. Cao, D. Sun, Z. Zhang, Y. Wang, Y. Wen, Y. Yang and T. Lyu, Sustainable Chromium (VI) Removal from Contaminated Groundwater Using Nano-Magnetite-Modified Biochar via Rapid Microwave Synthesis, *Molecules*, 2021, **26**, 103.

65 F.-X. Dong, L. Yan, X.-H. Zhou, S.-T. Huang, J.-Y. Liang, W.-X. Zhang, Z.-W. Guo, P.-R. Guo, W. Qian, L.-J. Kong, W. Chu and Z.-H. Diao, Simultaneous adsorption of Cr(VI) and phenol by biochar-based iron oxide composites in water: Performance, kinetics and mechanism, *J. Hazard. Mater.*, 2021, **416**, 125930.

66 A. T. Vo, V. P. Nguyen, A. Ouakouak, A. Nieva, B. T. Doma, H. N. Tran and H.-P. Chao, Efficient Removal of Cr(VI) from Water by Biochar and Activated Carbon Prepared through Hydrothermal Carbonization and Pyrolysis: Adsorption-Coupled Reduction Mechanism, *Water*, 2019, **11**, 1164.

67 V.-P. Dinh, P.-T. Nguyen, M.-C. Tran, A.-T. Luu, N. Q. Hung, T.-T. Luu, H. A. T. Kiet, X.-T. Mai, T.-B. Luong, T.-L. Nguyen, H. T. T. Ho, D.-K. Nguyen, D.-K. Pham, A.-Q. Hoang, V.-T. Le and T.-C. Nguyen, HTDMA-modified bentonite clay for effective removal of Pb(II) from aqueous solution, *Chemosphere*, 2022, **286**, 131766.

68 N. Liu, Y. Zhang, C. Xu, P. Liu, J. Lv, Y. Liu and Q. Wang, Removal mechanisms of aqueous Cr(VI) using apple wood biochar: a spectroscopic study, *J. Hazard. Mater.*, 2020, **384**, 121371.

69 D. Park, Y.-S. Yun and J. M. Park, Mechanisms of the removal of hexavalent chromium by biomaterials or biomaterial-based activated carbons, *J. Hazard. Mater.*, 2006, **137**, 1254–1257.

70 M. Gierada, F. De Proft, M. Sulpizi and F. Tielens, Understanding the Acidic Properties of the Amorphous Hydroxylated Silica Surface, *J. Phys. Chem. C*, 2019, **123**, 17343–17352.

71 E. A. Assirey and L. R. Altamimi, Chemical analysis of corn cob-based biochar and its role as water decontaminants, *J. Taibah Univ. Sci.*, 2021, **15**, 111–121.

72 L. Ma, N. Chen and C. Feng, Performance and enhancement mechanism of corncob guiding chromium (VI) bioreduction, *Water Res.*, 2021, **197**, 117057.

73 M. Ghanbarian, R. Nabizadeh, S. Nasseri, F. Shemirani, A. H. Mahvi, M. H. Beyki and A. Mesdaghinia, Potential of amino-riched nano-structured MnFe$_2$O$_4$@cellulose for biosorption of toxic Cr (VI): Modeling, kinetic, equilibrium and comparing studies, *Int. J. Biol. Macromol.*, 2017, **104**, 465–480.

74 Y. Bagbi, A. Sarswat, D. Mohan, A. Pandey and P. R. Solanki, Lead and Chromium Adsorption from Water using L-Cysteine Functionalized Magnetite (Fe$_3$O$_4$) Nanoparticles, *Sci. Rep.*, 2017, **7**, 7672.

75 V.-P. Dinh, T. D. Xuan, N. Q. Hung, T.-T. Luu, T.-T.-T. Do, T. D. Nguyen, V.-D. Nguyen, T. T. K. Anh and N. Q. Tran, Primary biosorption mechanism of lead (II) and cadmium (II) cations from aqueous solution by pomelo (Citrus maxima) fruit peels, *Environ. Sci. Pollut. Res.*, 2021, **28**, 63504–63515.